A&A 471, 193–204 (2007)
DOI: 10.1051/0004-6361:20065675

Astronomy & Astrophysics

Enrichment of the interstellar medium by metal-rich droplets and the abundance bias in H II regions

G. Stasińska[1], G. Tenorio-Tagle[2], M. Rodríguez[2], and W. J. Henney[3]

[1] LUTH, Observatoire de Paris, CNRS, Université Paris Diderot, Place Jules Janssen, 92190 Meudon, France
e-mail: grazyna.stasinska@obspm.fr
[2] Instituto Nacional de Astrofísica Óptica y Electrónica, AP 51, 72000 Puebla, Mexico
[3] Centro de Radioastronomía y Astrofísica, Universidad Nacional Autónoma de México, Campus Morelia, Apartado Postal 3-72, 58090 Morelia, Mexico

Received 23 May 2006 / Accepted 25 May 2007

ABSTRACT

We critically examine a scenario for the enrichment of the interstellar medium (ISM) in which supernova ejecta follow a long (10^8 yr) journey before falling back onto the galactic disk in the form of metal-rich "droplets", These droplets do not become fully mixed with the interstellar medium until they become photoionized in H II regions. We investigate the hypothesis that the photoionization of these highly metallic droplets can explain the observed "abundance discrepancy factors" (ADFs), which are found when comparing abundances derived from recombination lines and from collisionally excited lines, both in Galactic and extragalactic H II regions. We derive bounds of 10^{13}–10^{15} cm on the droplet sizes inside H II regions in order that (1) they should not have already been detected by direct imaging of nearby nebulae, and (2) they should not be too swiftly destroyed by diffusion in the ionized gas. From photoionization modelling we find that, if this inhomogeneous enrichment scenario holds, then the recombination lines strongly overestimate the metallicities of the fully mixed H II regions. The abundances derived from collisionally excited lines also suffer some bias, although to a much lesser extent. In the absence of any recipe for correcting these biases, we recommend the discarding of all objects showing large ADFs from studies of galactic chemical evolution. These biases must also be kept in mind when comparing the galactic abundance gradients for elements derived from recombination lines with those derived from collisionally excited lines. Finally, we propose a set of observations that could be undertaken to test our scenario and improve our understanding of element mixing in the ISM.

Key words. galaxies: abundances – galaxies: ISM – ISM: abundances – ISM: H II regions

1. Introduction

The detailed process of enrichment of the interstellar medium (ISM) by products arising from supernovae explosions and stellar winds is far from being fully understood (see review by Scalo & Elmegreen 2004). Many mechanisms are likely to be at work on different scales, both in time and in space (see, e.g., Bateman & Larson 1993; Roy & Kunth 1995; Tenorio-Tagle 1996; de Avillez & Mac Low 2002).

The present-day chemical composition of the ISM is derived from the analysis of the chemical abundances of H II regions. In such analysis, it is always assumed that H II regions are chemically homogeneous. So far, 2D and 3D spectroscopy of H II regions has not revealed the existence of zones with significantly different abundances within the same H II region, except in the case of NGC 5253, which shows some local N enhancement (Walsh & Roy 1989; Kobulnicky et al. 1997; López-Sánchez et al. 2007). On the other hand, chemical inhomogeneities occuring on scales smaller than the spatial resolution would pass unnoticed when comparing spectra of neighbouring zones.

There is, however, a way to unravel the presence of small-scale abundance inhomogeneities in H II regions. This is by comparing the abundances derived by traditional methods, i.e. from collisionally excited lines (CELs), to those obtained from optical recombination lines (ORLs) in the same spectrum. CELs are preferentially emitted in zones of high electron temperature and low metallicity, while ORLs are preferentially formed in zones of low electron temperature and high metallicity. So far, ORLs have been observed in only a few H II regions. They systematically lead to an abundance discrepancy factor (ADF)[1] larger than one. This has first been interpreted as due to temperature fluctuations within the H II regions (Peimbert et al. 1993; Peimbert 2003; Esteban et al. 1998, 1999a,b, 2002, 2004). However, Tsamis et al. (2003) consider that temperature fluctuations alone cannot be the cause of the observed discrepancies, since in that case oxygen abundances derived from far-infrared lines should be close to the high values obtained from optical recombination lines, and this is not the case (however, aperture problems are difficult to deal with, see García-Rojas et al. 2006). Tsamis et al. argue for the existence of a hitherto unseen component in H II regions, consisting of cold, metal-rich ionized parcels of gas. In fact, chemical inhomogeneities have been proposed for over a decade to explain the ORL/CEL discrepancy in planetary nebulae (Torres-Peimbert et al. 1990; Liu et al. 2000, 2004), but such an interpretation in the case of H II regions has appeared only recently (Tsamis et al. 2003; Tsamis & Péquignot 2005). Of course, chemical inhomogeneities in H II regions and planetary nebulae must have a very different origin. Note that invoking chemical inhomogeneities accounts at the same time for the origin of temperature fluctuations, which otherwise are

[1] The abundance disprepancy factor (ADF; Tsamis et al. 2004) of an ion is defined as the ratio of its abundance as derived from the intensities of ORLs to that derived from CELs.

difficult to explain quantitatively (see Stasińska 2007, and references therein).

In this article, we explore the possibility that the ADFs measured in H II regions result, as suggested by Tsamis et al. (2003, 2005), from the presence of metal-rich "droplets"[2] as predicted in the scenario of Tenorio-Tagle (1996; hereafter referred to as T-T96; see also Stasińska et al. 2007) for the enrichment of the ISM by Type II supernovae. Note that, up to now, reliable abundance discrepancy factors in H II regions have been measured only for oxygen. For simplicity, we will then consider only oxygen in this paper. Section 2 reviews the framework that accounts for the origin of such inhomogeneities in H II regions and evaluates their survival time-scale until full mixing with the ISM. This section gives also some observational arguments in support of the model. Section 3 estimates how much matter can be expected in the form of metal-rich droplets. Section 4 discusses the ORL/CEL discrepancy in H II regions in the context of metal-rich droplets. Section 5 presents some final comments and prospects.

2. Metal-rich droplets in H II regions

2.1. Formation of the droplets

The scenario proposed by T-T96 accounts for the fact that the ejecta from type II supernovae (SNe) ought to follow a long excursion into the galactic environment before they are able to mix with the ISM. The excursion is promoted by the clustering of massive stars and thus of type II SNe, which, being correlated in space and time, force the violently ejected matter to generate large-scale superbubbles. These are able to exceed the thickness of galactic disks and burst into the haloes of the host galaxies, while displacing and locking the surrounding ISM into kpc-size expanding supershells. Such remnants, driven by the hot superbubble interior grow for as long as massive stars continue to release their metals, until the last 8 $M_\odot$ star belonging to the star cluster or OB association completes its evolution (∼40 Myr). During this time, the metals injected into superbubbles have enough time to mix with the matter from stellar winds as well as with the matter thermally evaporated into the superbubbles from their surrounding outer supershells. Mixing within the superbubble interior is strongly favored by the high temperatures ($T \sim 10^6$–10^7 K) and high sound speeds and by the stirring caused by the bursting of more SNe. However, the remaining ISM, being out of contact with the superbubble interior, is left uncontaminated by the products of the evolving star cluster. After the last SN explosion, the low density within the superbubble interior ($n \sim 10^{-2}$–10^{-3} cm^{-3}) delays the impact of radiative cooling ($t_\Lambda \sim kT/(\Lambda n) \sim 10^8$ yr; where Λ is the cooling rate and k the Boltzmann constant). Note also that radiative cooling does not occur at the same rate within the entire volume of the superbubble, but rather zones with a higher density will cool faster than their surroundings. Such a situation has been shown to lead, in other astronomical circumstances such as galaxy formation or globular cluster formation (see Zel'dovich & Raizer 1966; Vietri & Pesci 1995), to multiple re-pressurising shocks which in our scenario would lead to the formation of small, dense "cloudlets" of metal-rich gas, in pressure equilibrium with the remaining hot gas. The high density of the cloudlets causes them to recombine, further reducing their temperature. The cold cloudlets would inevitably begin to fall towards the disk of the galaxy under the action of gravity. As they fall through the lighter interstellar medium, they will be subject to various instabilities, such as Rayleigh-Taylor and Kelvin-Helmholtz (e.g., Różyczka & Tenorio-Tagle 1985; Schiano et al. 1995), which will lead to their breakup into a swarm of minute droplets.

The overall outcome of such a fountain with a spray (as described by Scalo & Elmergreen 2004) is a large-scale dispersal of the matter processed by the star cluster over a large (kpc-scale) galactic volume, a volume much larger than the size of the stellar association. This is very different from other fountain models in which the hot gas rises to great altitudes (∼3 kpc) above the galactic plane to then cool all at once (see Kahn 1991). Such fountains would lead to massive giant clouds falling unimpeded towards the disk of galaxies. Note also that none of those models have addressed the mixing of metals with the ISM. On the other hand, the fountain with a spray of T-T96, predicts a stratus of dense, highly metallic and perhaps molecular droplets interspersed in the galactic ISM, wherever it had rained. Once this happens, the droplets are to participate in the general motion of clouds and intercloud medium promoted by galactic rotation and stellar activity, as envisaged by Roy & Kunth (1995). This is to lead to an even larger dispersal, although not to mixing of the metals with the ISM. For total mixing a new episode of stellar formation seems required as this will cause a thorough dissemination of the metals into the ISM enhancing its metallicity. This is primarily due to the UV radiation field, able to disrupt molecules and ionize the droplets and their surroundings, while generating multiple localized champagne flows (Tenorio-Tagle 1979) and with them the stirring to promote a rapid mixing within the ionized volume.

2.2. Survival of the droplets in H II regions

When the droplets are ionized, they will quickly (on order of a sound-crossing time) reestablish pressure balance with their surroundings. The two processes that will tend to disperse the high concentration of metals in the droplets are molecular diffusion and turbulent mixing.

The strong gradient in the concentration of oxygen ions between the droplets and the surrounding gas will eventually be diffused away due to the collisional random walks of the particles. The time required for diffusion through a distance L is of order

$$t_\mathrm{d} = L^2/D, \tag{1}$$

where D is the diffusion coefficient, which can be considered as the product of the root-mean-square particle velocity and the mean-free path between collisions (e.g., T-T96). For the diffusion of O^{++} ions moving in a field of H^+ ions, D can be calculated from the formulae presented in Oey (2003) as

$$D = 1.04 \times 10^{17} T_4^{5/2} n^{-1} f^{-1} \text{ cm}^2 \text{ s}^{-1}, \tag{2}$$

where T_4 is the gas temperature in units of 10^4 K, n is the hydrogen ion density, and $f = 1 + 0.029 \log T_4 - 0.010 \log n$. The resultant diffusion time is

$$t_\mathrm{d} = 3.05 \times 10^5 L_{15}^2 n f T_4^{-5/2} \text{ years}, \tag{3}$$

where L_{15} is the length scale in units of 10^{15} cm. Adopting characteristic values of density and temperature for O-rich droplets in pressure equilibrium ($n = 1000$ cm^{-3}, $T_4 = 0.6$, see Sect. 4),

[2] The word "droplets" is used in this paper with the same meaning as in Tenorio-Tagle (1996). It does not imply that they are in liquid form, but merely that they are of lower temperature and higher density than their surroundings.

we find $t_d = 10^9 L_{15}^2$ years. Therefore, metal-rich droplets as small as 10^{14} cm can survive over the entire lifetime of a typical H II region, but smaller droplets would be erased on smaller timescales and therefore would not contribute to the spectrum of any but the youngest H II regions. The corresponding mass of each droplet would be $\sim 10^{-11}\ M_\odot$. However, it is possible that disordered magnetic fields in the ionized gas might increase the diffusion time still further and allow smaller droplets to survive.

Discounting this last proviso, we have a rather stringent condition on the properties of the droplets: a physical size of 10^{14} cm corresponds to an angular size of $0.015''$ at the distance of the Orion nebula. Hence, droplets that are only a few times larger than this size may in principle be resolvable via direct imaging with the *Hubble Space Telescope*. There is already some observational evidence that inhomogeneities may indeed be present at this scale (O'Dell et al. 2003)

Diffusion by turbulent motions can be treated in a similar way. Assuming turbulent eddies of velocity $v_{\rm turb}$ and size $\ell_{\rm turb}$, then for times less than the coherence or turnover time, $\ell_{\rm turb}/v_{\rm turb}$, matter is simply advected at a speed $v_{\rm turb}$ and so the effective diffusion coefficient grows linearly with time. For $t > \ell_{\rm turb}/v_{\rm turb}$, on the other hand, the diffusion coefficient saturates at a constant value:

$$D_{\rm turb} = \ell_{\rm turb} v_{\rm turb}. \quad (4)$$

However, this equation only gives the rate of *dispersal* of the metal-rich gas by the turbulent eddies (Klessen & Lin 2003), but does not directly address the physical *mixing* of the two phases (de Avillez & Mac Low 2002). Mere dispersal of the droplets is not enough to destroy their physical integrity and distinctive temperature. Instead, it is necessary for the turbulent eddies to stretch and distort the droplets, so as to steepen the concentration gradients until they reach a level at which molecular diffusion can occur (see above). The relevant timescale for this process can be derived from the exponential stretching of fluid elements by the turbulent shear (Pan & Scalo 2007) as

$$t_{\rm mix} \sim t_{\rm d} \ln \mathcal{P}. \quad (5)$$

In this equation, $t_{\rm d}$ is the turbulent diffusion timescale calculated using Eq. (4) with $\ell_{\rm turb} = L$ (only those turbulent motions on the same scale as the droplets can efficiently distort them) and $\mathcal{P} = D_{\rm turb}/D$ is the Péclet number of the turbulence, with D given by Eq. (2). If turbulence of velocity v' is driven at some large scale ℓ', then the turbulent motions at a smaller scale $\ell_{\rm turb}$ have velocity $v_{\rm turb} = v'(\ell_{\rm turb}/\ell')^a$, where $a = 1/3$ for incompressible Kolmogorov turbulence (applicable to subsonic flows) and $a = 1/2$ in the limit of highly supersonic turbulence. The turbulence in H II regions is likely driven by the mutual interactions of multiple transonic photoablation flows (Mellema et al. 2006; Henney 2006), with Mach numbers in the range 2–4 and at scales of 0.1 to 1 parsec. We therefore find a turbulent mixing time of

$$t_{\rm mix} = 12,600 (L_{15} \ell'_{18})^{1/2} v_{10}^{-1} g \text{ years}, \quad (6)$$

where ℓ'_{18} and v_{10} are the scale and velocity of the turbulent driving in units of 10^{18} cm and 10 km s^{-1}, respectively, and $a = 1/2$ is assumed[3]. This result implies that turbulent mixing is efficient on timescales shorter than those characteristic of H II region evolution.

[3] The expression also includes the term $g = 1 + 0.034 \log n_3 f + 0.052 \log L_{15} - 0.017 \log \ell'_{18} - 0.086 \log T_4$, but this will always be close to unity.

Since the turbulent $t_{\rm d}$ decreases as the droplet size is reduced, the turbulence will quickly fragment the droplets to such an extent that the molecular diffusion also becomes efficient (at scales of order 10^{12} cm), at which point chemical mixing will be complete. The long-term survival of the droplets in the H II region therefore depends critically on the avoidance of turbulence.

The extent to which turbulence is present in H II regions is somewhat controversial. It is certainly the case that the internal kinematics of H II regions are highly irregular, with significantly non-thermal linewidths (O'Dell & Castañeda 1987). However, it is unclear whether this represents true hydrodynamical turbulence, or simply the superposition of multiple velocity components, each one of which arises in an ordered flow. Recent simulations of H II region evolution in a clumpy molecular cloud (Mellema et al. 2006) indicate that the "chaotic" velocity field is largely the result of inward-pointing photoablation flows, which form wherever the outward propagation of the ionization front is detained by a dense neutral condensation. These flows shock against one another in the interior of the H II region, which does become truly turbulent. However, it is found that 10–30% of the [O III] emission comes from the non-turbulent flows closer to the ionization front. A similar result was derived analytically by Henney (2003), who showed that the surface brightness of such photoablation flows is proportional to the linear size of the cavities that they carve out of the H II region, which in turn is a function of the scale of the irregularities in the front. Flows from condensations with size >10% the radius of the H II region will have a brightness comparable to that of the entire region. Both these studies considered only H II regions with globally closed geometries, although it is likely that many optically visible regions are instead globally open champagne flows (e.g., Tenorio-Tagle 1979; Henney et al. 2005), which would tend to increase the relative contribution of the photoevaporation flows to the total emission. On the other hand, the interaction of the stellar wind from the ionizing star with the other flows (e.g., García-Arredondo et al. 2001) may be an additional source of turbulence, as may instabilities of the ionization front (García-Segura & Franco 1996; Williams 1999, 2002). Here we thus assume that turbulence and molecular diffusion act very effectively within the HII region volume, causing a thorough mixing and homogeinizing of the ionized gas. However, we also assume that at all times there are new metal-rich droplets traversing the ionization front into the HII region.

2.3. Observational considerations

There are several further observational facts that lend support to the droplet scenario, facts that ought to be taken into consideration by other possible explanations of how the mixing of heavy elements with the ISM takes place. Regarding abundances in H II regions the issues are:

Given the lifetime of type II SN progenitors (up to several 10^7 yr), it is obvious that the metals expected from recent bursts of stellar formation (age $\sim$ a few 10^6 yr) have not yet been released and thus the detected abundances in H II regions reflect the production, dispersal and mixing of heavy elements ejected by former stellar generations.

This result is supported by the work of Simón-Díaz et al. (2006) who measured the oxygen abundance in the atmospheres of three OB stars in the Orion nebula and found that it is indistinguishable, within errors, from the one determined by Esteban et al. (2004) for the surrounding H II region. Thus the material gathered by the star(s) during collapse and the star formation process had the same contaminating metals and in the same

proportion – given by Eq. (22) – as those detected in their photoionized volumes.

Low mass galaxies such as I Zw 18 (Vílchez & Iglesias-Páramo 1998; Legrand 2000), II Zw 40, NGC 4214 (Kobulnicky & Skillman 1996), NGC 1569 (Devost et al. 1997), Sextans A and B (Kniazev et al. 2005), in which abundances have been measured in several locations all present very uniform metal abundances within their ionized volumes. Given the size of these H II galaxies (≥1 kpc), these facts imply a very even large-scale dispersal of the metals from former stellar generations. Scalo & Elmegreen (2004) summarize the evidence for abundance variations in the ISM of our Galaxy, concluding that the gas is well-mixed on scales from 1 to 100 parsec. Note that the inhomogeneities posited in the scenario considered in this paper are on much smaller scales.

Abundances in the ISM can also be obtained from the absorption lines produced by the H I envelopes that surround H II regions. These derivations are difficult and uncertain and require very high resolution far-UV spectroscopy. The more reliable, recent results in external galaxies (e.g. Aloisi et al. 2003; Lebouteillier et al. 2004) indicate an oxygen abundance in the H I regions several times lower than in the H II regions (although this is not always the case, see Thuan et al. 2005). A systematic difference between abundances in H II and H I regions has many possible explanations. One of them is that abundance determinations using absorption and emission lines have significantly different biases in the case of abundance inhomogeneities.

Finally, using long-slit spectroscopy of the Orion nebula, Rubin et al. (2003) have shown the presence of temperature fluctuations on a scale of 0.5″. In the same object, from the ratio of [O III] λ4363 and [O III] λ5007 *Hubble Space Telescope* images, O'Dell et al. (2003) found small scale temperature fluctuations of ±400 K on the 10″ scale, but with most power being at smallest scales: 0.1″, i.e., 6.45×10^{14} cm. O'Dell et al. (2003) say that shadows behind clumps close to the ionization fronts can partly account for the observed temperature fluctuation, but an additional cause is needed. As a matter of fact, these observed fluctuations could be due to our metal-rich droplets. The dominant scale of the observed fluctuations is tantalisingly close to the droplet sizes derived in Sect. 2.2. Correlations of these observed fluctuations with surface brightness would give a hint on whether our interpretation is correct.

3. How much does it rain?

In order to see what mass fraction of oxygen can be expected in the droplets, here we consider a simple scheme for the life cycle of metal-rich droplets assuming a steady state.

3.1. Formal derivation

If one assumes that all the oxygen ejected by massive stars eventually rains down in the form of highly metallic droplets, the rainfall rate of oxygen in drops at a given time t is given by:

$$R(t) = e_*(\mathrm{O})\,\dot{\Sigma}_*(t-\Delta t), \tag{7}$$

where $e_*(\mathrm{O})$ is the mass fraction of all stars formed that is ejected as oxygen by SNe, and $\dot{\Sigma}_*(t-\Delta t)$ is the star formation rate (SFR) per unit area at $t-\Delta t$, with $\Delta t \sim 10^8$ yr, the time needed for SNe ejecta to travel through the halo and return to the disk. The droplets end up being homogeneously distributed in the ISM, to then be fully processed while enhancing the metallicity of newly formed stars and of their photoionized surrounding gas, every time that they participate in new bursts of stellar formation.

If X_i is the mass of gas that is ionized per unit mass of stars formed, the fraction of gas ionized or incorporated into stars per unit time is $I(t) = (X_\mathrm{i}+1)\,\dot{\Sigma}_*(t)/\Sigma_\mathrm{ISM}(t)$, where Σ_ISM is the surface density of gas. The rate per unit area at which oxygen is released from the droplets to the ISM is:

$$I(t)\,\Sigma_\mathrm{D}(\mathrm{O};t) = \frac{(X_\mathrm{i}+1)\,\dot{\Sigma}_*(t)}{\Sigma_\mathrm{ISM}(t)}\,\Sigma_\mathrm{D}(\mathrm{O};t), \tag{8}$$

where $\Sigma_\mathrm{D}(\mathrm{O};t)$ is the oxygen mass in droplets per unit area at time t. The time variation of $\Sigma_\mathrm{D}(\mathrm{O};t)$ is then:

$$\frac{\mathrm{d}\Sigma_\mathrm{D}(\mathrm{O};t)}{\mathrm{d}t} = R(t) - I(t)\,\Sigma_\mathrm{D}(\mathrm{O};t). \tag{9}$$

If one considers a time interval $t-t_0$ during which $\dot{\Sigma}_*(t-\Delta t)$, $\dot{\Sigma}_*(t)$, and $\Sigma_\mathrm{ISM}(t)$ are approximately constant, Eq. (9) can be integrated to give:

$$\Sigma_\mathrm{D}(\mathrm{O};t) = \left(\Sigma_\mathrm{D}(\mathrm{O};t_0) - \frac{R}{I}\right)\mathrm{e}^{-I(t-t_0)} + \frac{R}{I}. \tag{10}$$

The drops processing timescale is thus:

$$\tau_\mathrm{D} = \frac{1}{I} = \frac{\Sigma_\mathrm{ISM}}{(X_\mathrm{i}+1)\dot{\Sigma}_*(t)}. \tag{11}$$

If we take $X_\mathrm{i} = 9$ masses of ionized gas per unit mass in new stars (Williams & McKee 1997), with $\Sigma_\mathrm{ISM} \simeq 10\ M_\odot\ \mathrm{pc}^{-2}$ (see Fig. 16 of Mollá & Díaz 2005) and $\dot{\Sigma}_* = 7.5\ M_\odot\ \mathrm{pc}^{-2}\ \mathrm{Gyr}^{-1}$ (McKee & Williams 1997) in the solar neighbourhood, $\tau_\mathrm{D} \simeq 130$ Myr. And for $t-t_0$ equal to 2–3 times the processing timescale τ_D, we get from Eq. (10):

$$\Sigma_\mathrm{D}(\mathrm{O};t) \simeq \frac{R}{I} = \frac{e_*(\mathrm{O})\,\dot{\Sigma}_*(t-\Delta t)\,\Sigma_\mathrm{ISM}}{(X_\mathrm{i}+1)\,\dot{\Sigma}_*(t)}, \tag{12}$$

and if the SFR has been approximately constant for the last one or few Gyr (probably a good approximation to within a factor of 2 for our own Galaxy – see Fig. 15 of Mollá & Díaz 2005):

$$\Sigma_\mathrm{D}(\mathrm{O};t) = \frac{e_*(\mathrm{O})\,\Sigma_\mathrm{ISM}}{(X_i+1)}. \tag{13}$$

The surface density of gas in the droplets with respect to the surface density of gas in the ISM is

$$X = \frac{\Sigma_\mathrm{D}}{\Sigma_\mathrm{ISM}} = \frac{\Sigma_\mathrm{D}(\mathrm{O};t)}{\Sigma_\mathrm{ISM}(\mathrm{O};t)}\,\frac{Z_\mathrm{ISM}(\mathrm{O})}{Z_\mathrm{D}(\mathrm{O})}, \tag{14}$$

where $Z_\mathrm{D}(\mathrm{O})$ and $Z_\mathrm{ISM}(\mathrm{O})$ are the oxygen mass fractions in the droplets and in the ISM, respectively.

If we define the parameter η by:

$$\eta = \frac{e_*(\mathrm{O})}{(X_\mathrm{i}+1)\,Z_\odot(\mathrm{O})}, \tag{15}$$

it follows from Eqs. (13) and (14) that:

$$X = \frac{\eta}{Z_\mathrm{D}(\mathrm{O})/Z_\odot(\mathrm{O})}. \tag{16}$$

In first approximation, the value of η is not expected to vary strongly with metallicity, so the value of X is roughly inversely proportional to the metallicity of the droplets.

Table 1. Mass fraction of all stars formed that is ejected as oxygen.

IMF[a]	$Z/Z_\odot$	e_*(O)	Ref.
Scalo	0.1	0.0020–0.0024	1
Scalo	1	0.0022–0.0027	1
Scalo	0.02	0.0040	2
Scalo	1	0.0039	2
Salpeter	0.1	0.0052–0.0062	1
Salpeter	1	0.0056–0.0070	1
Salpeter	0.02	0.0104	2
Salpeter	1	0.0100	2
Kroupa	0.1	0.0092–0.0110	1
Kroupa	1	0.0099–0.0120	1
Kroupa	0.02	0.0184	2
Kroupa	1	0.0177	2

1- Woosley & Weaver (1995); 2- Portinari et al. (1998). [a] The IMF slopes are those of Scalo (1986) – as given in Lanfranchi & Matteucci (2003) –, Salpeter (1955), and Kroupa (2001).

3.2. Numerical estimates

Neither the value of e_*(O) nor the value of X_i are well-known. In Table 1, we show different estimations of e_*(O). This is approximately equal to the mass fraction of oxygen ejected by stars of all masses, since the contribution of intermediate mass stars is negligible. The values shown in Table 1 are based on different sets of calculations of stellar yields and on different stellar initial mass functions. There is presently no consensus on which are the most realistic values and chemical evolution models of galaxies have been constructed exploring different sets of yields and initial mass functions (e.g., Portinari et al. 1998; Henry et al. 2000; Chiappini et al. 2003; Francois et al. 2004). In Table 1, the values of e_*(O) range between 0.002 and 0.018. They have been computed for a lower stellar mass of $M_{\rm down} = 0.1\ M_\odot$ and an upper stellar mass of $M_{\rm up} = 120\ M_\odot$. Adopting larger values of $M_{\rm down}$ but maintaining the same initial mass functions would lead to somewhat larger values of e_*(O) (e.g. 0.015 for $M_{\rm down} = 0.3\ M_\odot$ instead of 0.01 for $M_{\rm down} = 0.1\ M_\odot$ in the case of the yields of Portinari et al. 1998 with the Salpeter initial mass function).

Concerning X_i, the situation is probably even more complex, because an estimate of this parameter involves a representation of the structure of the ISM on different scales and a knowledge of all the forces at play, in addition to the IMF description. Using a simple argument of ionization balance, Izotov et al. (2006) derive $X_i = 360/n$, where n is the ionized gas density. So, for a density of 300 cm^{-3}, X_i would be close to 1. In a comprehensive study of the evolution of molecular clouds in the Galaxy, Williams & McKee (1997) give $X_i = 9$ while from the work of Franco et al. (1994) one derives $X_i \sim 25$. The parameter X_i is likely to change with metallicity due to a varying amount of ionizing photons absorbed by dust or to a change in the hardness of the ionizing radiation field.

Figure 1 shows the variations of X as a function of Z_D for $\eta = 0.17$, our working value in the remaining of the paper (which corresponds to e_*(O) = 0.01 and $X_i = 9$).

Finally, note that a change by a given factor in the star formation rate between $t - \Delta t$ and t would change X by the same factor.

4. Metal-rich droplets and the ORL/CEL discrepancy

4.1. ADFs measured in H II regions

Table 2 lists the values of the densities, temperatures and abundance discrepancy factors ADF(O^{++}) found in the literature for Galactic and extragalactic H II regions. The temperatures derived from Balmer jump, T_e(BJ), are not available for all cases and bear generally significant uncertainties. It is however clear that they are, on average, smaller than those derived from [O III] λ4363/5007 line ratios, T_e[O III]. The listed ADFs are equal to the ratio of the value of the O^{++} abundance derived from [O III] λ5007 to the one derived from O II recombination lines, using T_e[O III] in both cases. These ADFs were obtained from several recombination lines of O II and the forbidden line [O III] λ5007, using the temperature T_r[O III] derived from the [O III] λ4363/5007 ratio. The values of ADF(O^{++}) are found to be around 2, over a large range of H II region metallicities: $12 + \log(O/H) = 7.87$–8.56 (i.e., $Z = 0.15$ to $0.75\ Z_\odot$). However, note that the ADFs measured for most of the extragalactic H II regions in Table 1 and, in particular, for all the low metallicity objects ($12 + \log(O/H) < 8.3$) were derived using the O II lines of multiplet 1, and these lines can be severely affected by stellar absorption lines (Tsamis et al. 2003). This means that the ADFs could be much larger than 2 for these objects.

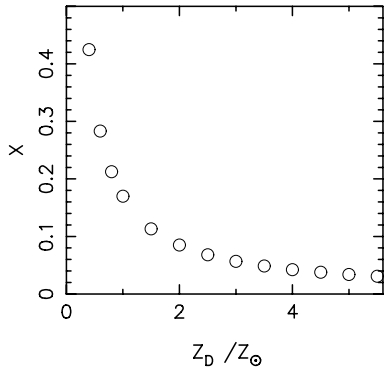

Fig. 1. The value of $X = M_D/M_{ISM}$ as a function of the metallicity of the droplets, assuming that $\eta = 0.17$ (see Eqs. (18) and (19) in text).

4.2. A simple expression for the ADF

To better understand what an ADF really is, we derive here an approximate expression for it in the case of a two-component toy model. In a medium characterized by an electron density n_e and an electron temperature T_e, the luminosity in an optically thin line arising from O^{++} ions is given by

$$L = N(O^{++}) n_e \epsilon(T_e), \tag{17}$$

where N(O^{++}) is the total number of O^{++} ions in the emitting volume, and $\epsilon(T_e)$ is the line emissivity, in erg cm^3 s^{-1}, which depends essentially on the electron temperature (for the sake of simplicity, we neglect the density dependence, as it is not important in the problem considered here). The expression for ADF(O^{++}) is then given by

$$\mathrm{ADF}(O^{++}) = \frac{L_{ORL}/\epsilon_{ORL}(T_e)}{L_{CEL}/\epsilon_{CEL}(T_e)}, \tag{18}$$

where T_e is taken equal to T_r[O III]. However, if within the emitting volume there are two different media with different physical parameters such as their metallicity, then

$$\mathrm{ADF}(O^{++}) = \frac{(L^a_{ORL} + L^b_{ORL})/\epsilon_{ORL}(T_e)}{(L^a_{CEL} + L^b_{CEL})/\epsilon_{CEL}(T_e)}, \tag{19}$$

where a and b refer to the two media, and T_e is here again equal to the temperature derived from the observations, T_r[O III]. In the

Table 2. Densities, temperatures, metallicities and ADFs measured in H II regions.

ID	n_e (cm^{-3})[a]	T_e[O III] (K)	T_e(BJ) (K)	12 + log(O/H)[b]	$Z/Z_\odot$[c]	ADF(O^{++})	Ref
Galactic H II regions							
M8	1750	8050 ± 700	–	8.41	0.52	2.0	1
	1800	8090 ± 140	7100^{+1250}_{-1000}	8.51	0.66	2.3	2
M 16	1120	7650 ± 250	5450 ± 820	8.56	0.74	2.8	3
M 17	860, 520	8120 ± 250, 8210 ± 250	–	8.53, 8.50	0.69, 0.65	1.8, 2.2	4
	600–1500	8200	7700	8.56	0.74	2.1	5
	470	8020 ± 170	–	8.52	0.68	1.9	2
M 20	270	7800 ± 300	6000 ± 1300	8.53	0.69	2.1	3
M 42	4000, 5700	8300 ± 210, 8350 ± 200	8730 ± 800, 8390 ± 800	8.47, 8.47	0.60, 0.60	1.3, 1.5	6
	–	–	–	8.52	0.68	1.3	5
	8900	8300 ± 40	7900 ± 600	8.51	0.66	1.4	7
NGC 3576	1300–2700	8850	8070	8.52	0.68	1.8	5
	2800	8500 ± 50	6650 ± 750	8.56	0.74	1.9	8
NGC 3603	5150	9060 ± 200	–	8.46	0.59	1.9	3
S311	310	9000 ± 200	9500 ± 900	8.39	0.50	1.9	9
Extragalactic H II regions							
LMC 30 Dor	370–1800	10100	–	8.34	0.45	2.0–2.7[d]	5
	316	9950 ± 60	9220 ± 350	8.33	0.44	1.6	10
LMC N11B	80–1700	9400	–	8.41	0.52	4.9–8.2[d]	5
NGC 604	≤100	8150 ± 150	–	8.49	0.63	1.6	11
NGC 2363	360–1200	15 700 ± 300	–	7.87	0.15	2.2	11
NGC 5253	370–610	10 940–12010	–	8.18–8.28	0.31–0.39	1.5–1.9	12
NGC 5461	300	8600 ± 250	–	8.56	0.74	1.9	11
NGC 5471	220–1150	14 100 ± 300	–	8.03	0.22	1.6	11
NGC 6822 V	175	11 900 ± 250	–	8.08	0.24	1.9	13
SMC N66	50–3700	12400	–	8.11	0.26	2.3	5

1- Esteban et al. (1999a); 2- García-Rojas et al. (2006b); 3- García-Rojas et al. (2006a); 4- Esteban et al. (1999b); 5- Tsamis et al. (2003); 6- Esteban et al. (1998); 7- Esteban et al. (2004); 8- García-Rojas et al. (2004); 9- García-Rojas et al. (2005); 10- Peimbert (2003); 11- Esteban et al. (2002); 12- López-Sánchez et al. (2007); 13- Peimbert et al. (2005) [a] The high values of the densities in the extragalactic H II regions mostly come from the [Ar IV] ratio and are very uncertain. [b] 12 + log(O/H) from forbidden lines. [c] the Solar oxygen abundance is taken from Allende Prieto et al. (2001). [d] In 30 Dor and N11B, the highest values of the ADFs include a correction for contamination by scattered light.

limiting case in which the medium b is too cold to contribute significantly to the CEL intensities (which is easy to achieve due to the very strong temperature dependence of the λ4363 and λ5007 lines), T_r[O III] is in fact the temperature of medium a. Using Eq. (17), Eq. (19) becomes:

$$\mathrm{ADF(O^{++})} = 1 + \frac{N^b(\mathrm{O^{++}})}{N^a(\mathrm{O^{++}})}\frac{n_e^b}{n_e^a}\frac{\epsilon_{\mathrm{ORL}}(T_e^b)}{\epsilon_{\mathrm{ORL}}(T_e^a)}, \quad (20)$$

or,

$$\mathrm{ADF(O^{++})} = 1 + \frac{x^b(\mathrm{O^{++}})}{x^a(\mathrm{O^{++}})}\frac{n_e^b}{n_e^a}\frac{Z^b}{Z^a}\frac{M^b}{M^a}\frac{\epsilon_{\mathrm{ORL}}(T_e^b)}{\epsilon_{\mathrm{ORL}}(T_e^a)}, \quad (21)$$

where x^a, x^b stand for the doubly ionized oxygen fractions, Z^a, Z^b are the O/H ratios (or "metallicites"), and M^a, M^b are the total hydrogen masses in zones a and b, respectively. Note that ϵ_{ORL} is an increasing function of Z via T_e, and $x(\mathrm{O^{++}})$ is a decreasing function of n_e due to recombination. The observed values of the ADFs in H II regions impose strong constraints on the parameters that come into play.

4.3. Photoionization modelling

We now simulate the situation described in Sect. 2 by a set of photoionization models. We consider three ionized components, each with its own metallicity: the highly metallic droplets, the background ISM, which is being ionized at the same time as the droplets, and the H II region into which the former two media have mixed. At each moment, a mass M_D of droplets with metallicity Z_D and a mass M_{ISM} from the ISM with metallicity Z_{ISM} are being ionized and will eventually result in a mass M_{HII} of ionized gas with metallicity

$$Z_{HII} = \frac{XZ_D + Z_{ISM}}{X+1}, \quad (22)$$

where $X = M_D/M_{ISM}$. Figure 2 shows Z_{HII} as a function of Z_D for $Z_{ISM} = 0.2$ and $0.6\ Z_\odot$, taking $\eta = 0.17$.

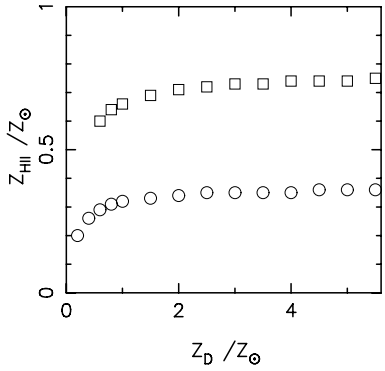

Fig. 2. The metallicity of the fully mixed H II region as a function of the metallicity of the droplets, for $Z_{ISM}/Z_\odot = 0.2$ (circles) and $Z_{ISM}/Z_\odot = 0.6$ (squares), assuming that $\eta = 0.17$ (see Sect. 3.1).

The real progression of the ionization front is complex, but the situation can be modelled in a simple way by considering that the ISM, the droplets and the fully mixed H II region, with typical densities n_{ISM}, n_D and n_{HII}, respectively, are impacted by the same ionizing radiation field. This implies that the droplets

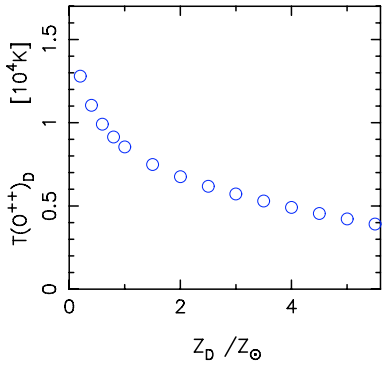

Fig. 3. The average temperature in the O^{++} zone of the droplets, as a function of the metallicity of the droplets.

do not have too large a covering factor so that the general ISM can be ionized (in principle, a situation where the droplets would completely block the ionizing photons is possible as well, but not considered in this paper).

Here we assume that any observation of an H II region encompasses zones close to the ionization front that have just been ionized and still have their initial metallicities Z_D and Z_{ISM}, and zones that have been ionized some time ago and have acquired, through the turbulent stirring promoted by well localized champagne flows (see Sect. 2), the metallicity Z_{HII} given by Eq. (22). We assume that this fully mixed gas contributes a fraction, F, of the total observed Hβ flux from the H II region. Note that the parameter F also accounts for the lifetime of the droplets once they are ionized.

For a given stellar radiation field, and a given value of η – as defined by Eq. (15) – the problem is entirely specified by the parameters F, Z_D and Z_{ISM}, and the densities of the three different media. We expect the densities n_{ISM} and n_{HII} to be of the same order of magnitude because the fully mixed ionized gas must be in rough pressure equilibrium with the ISM gas that has just been ionized and because temperature differences between the media are likely small, which is confirmed by our results shown in Figs. 4d and 5d. For the computations, inspired by the observed values listed in Table 2, we have taken $n_{ISM} = n_{HII} = 300\ cm^{-3}$. Since the droplets are more metallic than the ISM, their temperature must be lower, and thus we assumed the droplets to be denser than the background. We have considered various density contrasts and present results from calculations assuming $n_D = 1000\ cm^{-3}$. The computations were done with the code PHOTO (Stasinska 2005), taking for the ionizing radiation field that of a blackbody at a temperature $T_{eff} = 50\,000$ K. The inner radius of the models is the same for the three components, and has been chosen so that the ionization parameter at the inner radius, U, is equal to 10^{-2} both for the H II region and the ISM[4]. Figure 3 shows how the O^{++}-weighted temperature in the droplets decreases as a function of the droplet metallicity.

We computed models of the droplets with various values of Z_D, and models for the mixed H II region with Z_{HII} as given by Eq. (22), the value of X resulting from Eq. (16) for an adopted η of 0.17. We combined the photoionization models for the droplets, the ISM and the fully mixed H II region taking various values of F. We then applied to the resultant models the same techniques as an observer deriving T_r[O III], ADF(O^{++}), and the metallicities from the collisionally excited lines and recombination lines. We used exactly the same atomic data as for the photoionization models.

4.4. Discussion of the simulated observations

The number of parameters in this problem is large, and displaying our results for the entire parameter space would be cumbersome. Since the main goal of this paper is to investigate whether the ADFs observed in H II regions could indeed be the signature of the enrichment scenario proposed by T-T96, we will concentrate on a few plausible cases, and try to learn some lessons from them.

Figure 4 presents the results of simulations for $Z_{ISM} = 0.2\ Z_\odot$, taking $\eta = 0.17$ (the working value presented in Sect. 3.2). In all the nine panels the abscissa represents Z_D in solar units. The range of values for Z_D was inspired by the work of Silich et al. (2001) where the metallicity of the hot superbubble interior, resultant from the multiple SN explosions of an aging star cluster, was calculated. The various cases they considered (see their Fig. 6) encompass starbursts evolving in low and high metallicity galaxies and account for mass evaporation from the surrounding supershell into the hot superbubble interior. The final values, the metallicity of the matter that will eventually cool to compose the high metallicity droplets, range from 0.2 $Z_\odot$ to 5 $Z_\odot$. In the plots, simulations corresponding to an observation where $F = 0.1$ are represented by circles, those corresponding to $F = 0.5$ by squares, and those corresponding to $F = 0.9$ by triangles. Panel a shows the simulated ADF(O^{++}), panel b shows T_r[O III], panel c shows Z_{CEL}, the metallicity derived from collisionally excited lines. These three quantities represent "observables". The next panels show other results from the simulations, which shed some light on the behaviour of the "observables". Panel d shows $T(O^{++})_{HII}$, the O^{++}-weighted temperature in the fully mixed H II region (which, as can be seen by comparing panels b and d, is not identical to the temperature derived from the [O III] λ4363/5007 ratio). Panels e and f show the bias in the determination of the metallicity when using collisionally excited lines (Z_{CEL}/Z_{HII}) or recombination lines (Z_{ORL}/Z_{HII}). The computed values of Z_{CEL} and Z_{ORL} take into account the contribution of O^+, which has been evaluated from the [O II] λ3727 line using the temperature derived from the [N II] λ5755/6584 line ratio. Note that this procedure gives lower ORL abundances than the procedure used by most authors quoted in Table 2, who correct the temperature of the O^+ zone for temperature fluctuations using the scheme of Peimbert (1967). Panels g, h and i show the flux from the droplets in the [O III] λ4363, [O III] λ5007 and O II λ4651[5] lines, with respect to the total in these lines.

As expected, ADF(O^{++}) increases with Z_D, and, for a given Z_D, it is larger for smaller values of F. The computed Z_{CEL} also strongly depend on F. In other words, the computed metallicity is higher if the observation gathers less light from the fully mixed H II region with respect to the newly ionized gas. The behaviour of T_r[O III] is more intricate. As Z_D increases, the temperature in the drops becomes smaller, as seen in Fig. 3, due to the increased cooling by metals. One would expect T_r[O III] to decrease as Z_D increases. This is seen only at small values of Z_D. The behaviour of T_r[O III] is actually due to a subtle combination of various effects, linked to the temperatures in the three phases of our models and in the respective proportions of these phases in the resultant model. The temperature in the fully mixed H II region decreases slightly as Z_D increases, because Z_{HII} increases as

[4] We use the definition $U = Q_H/(4\pi R^2 n)$, where Q_H is the number of stellar ionizing photons, R is the distance to the star, and n is the gas density.

[5] Following the usual nomenclature for recombination lines, the O II λ4651 line is emitted by the recombining O^{++} ion.

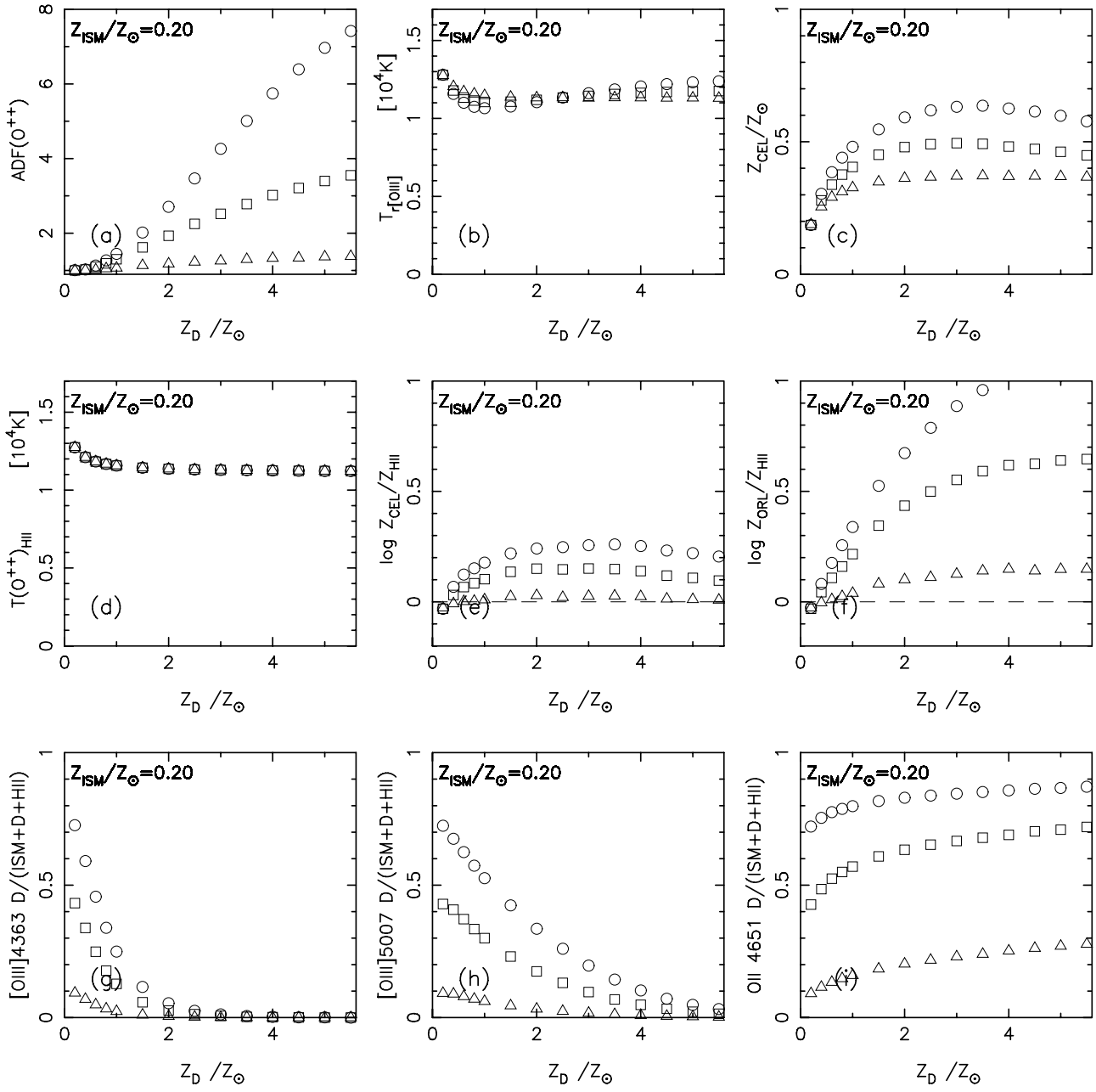

Fig. 4. Results of simulations for a series of models with $Z_{\rm ISM} = 0.2\ Z_\odot$ as a function of $Z_{\rm D}$, for various values of F and taking $\eta = 0.17$ (see Sects. 3.2 and 4.3). Circles: $F = 0.1$; squares: $F = 0.5$; triangles: $F = 0.9$. "Observables": **a**) ADF(O^{++}); **b**) $T_{\rm r}$[O III]; **c**) $Z_{\rm CEL}$ (see text). Other results of the simulations: **d**) $T(O^{++})_{\rm HII}$, **e**) $Z_{\rm CEL}/Z_{\rm HII}$, i.e., the metallicity bias when using [O III] λ5007 (see text) **f**) $Z_{\rm ORL}/Z_{\rm HII}$, i.e., the metallicity bias when using the O II λ4651 line to measure the oxygen abundance (see text); **g**), **h**) and **i**): the flux from the droplets in the [O III] λ4363, [O III] λ5007 and O II λ4651 lines, with respect to the total in these lines.

prescribed by Eq. (22), which accounts for mass and metal conservation. However Fig. 4g shows that the drops contribute less to the [O III] λ4363 flux than to the [O III] λ5007 flux, and thus, the [O III] λ4363/5007 ratio is larger when the contribution of the resultant H II region to [O III] λ5007 is smaller. The value of $Z_{\rm CEL}$ is not only related to the ADF, but also to the contribution of the O^+ zone. Therefore, the behaviour of $Z_{\rm CEL}$ with $Z_{\rm D}$ seen in Fig. 4c is not necessarily universal. A wide range of numerical models, with a better representation of the physical model and a better sampling of excitations conditions would be needed to draw some useful conclusions from the computed values of $Z_{\rm CEL}$.

Figure 5 is the same as Fig. 4, but now for simulations with $Z_{\rm ISM} = 0.6\ Z_\odot$. Qualitatively, it displays the same characteristics as Fig. 4, but with less extreme features. The ADFs(O^{++}) are here much smaller, because the temperature contrast between the metal-rich drops and the ISM is smaller. On the other hand, simulations with $Z_{\rm ISM}$ smaller than $0.2\ Z_\odot$, not shown here, lead to more extreme characteristics than displayed in Fig. 4.

The same set of figures for droplets with a density $n_{\rm D} = 3000$ instead of 1000 cm^{-3} are very similar to Figs. 4 and 5, but with smaller effects, due to the fact that gas is more recombined in the droplets than in the cases shown here. However, the density

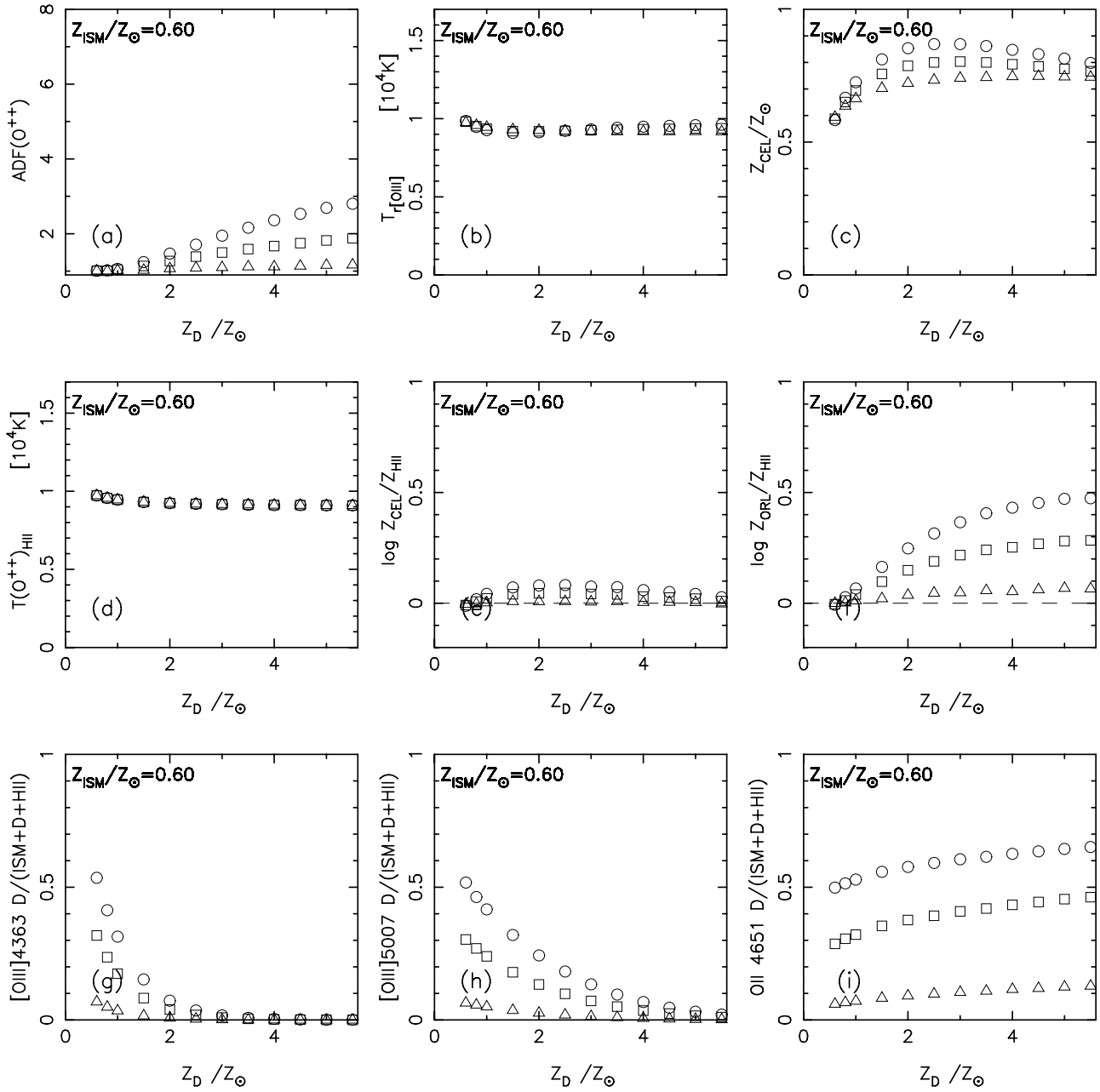

Fig. 5. Same as Fig. 2 but for models with $Z_{\rm ISM} = 0.6\ Z_\odot$.

effect is only slight, since, as seen in Eq. (21) the effects of density and recombination on ADF(O^{++}) tend to compensate.

Our computations were carried out with a given stellar radiation field and with a given ionization parameter. We do not expect large changes in our results when modifying the stellar radiation field or ionization parameter within the limits relevant to bright H II regions. The average effective temperature does not change much from one object to another, and is a second order parameter in our problem. The ionization parameter can be different from object to object, but the ADFs are abundance ratios of the same ion, and thus are not dependent on the ionization parameter to first order. Test computations have confirmed this view.

The most important parameters are $Z_{\rm D}$ and F (which are varied in the plots presented in Figs. 4 and 5) and our parameter η, which, from considerations in Sect. 3.2, has a large range of possible values.

Table 3 summarizes our knowledge on the range of parameters entering the model.

Table 3. Expected range of parameters entering the model.

Parameter	Values	Argumentation
e_*(O)	0.002–0.018	Table 1
$X_{\rm i}$	1 ?–25 ?	see Sect. 3.2
$Z_{\rm D}$	$Z_{\rm ISM}$–10 $Z_\odot$?	Silich et al. (2001)
$n_{\rm HII}$	100–5 000 cm^{-3}	Table 2
$n_{\rm ISM}$ /$n_{\rm HII}$	$\simeq$1	see Sect. 4.3
$n_{\rm D}$ /$n_{\rm ISM}$	3–30	rough pressure equilibrium
U	10^{-3}–10^{-1}	Stasińska & Leitherer (1996)
$T_{\rm eff}$	35 000–55 000 K	massive stars
F	0–1	see Sect. 4.4

4.5. What the confrontation between computed ADFs and observed ADF tells us

Let us now compare the simulations shown in Figs. 4 and 5 with the observations. The Galactic and Magellanic Clouds nebulae listed in Table 2 have diameters of (10–50)′ while the slits have widths of (1–3)″, so that the spectroscopic observations cover a tiny fraction of the objects, and the contribution from the fully mixed H II region is likely small. The remaining extragalactic objects are smaller, with angular radii of (10–100)″, so the contribution of the fully mixed H II region is more important, however still small. We thus believe that the models to be compared to the available observations are those corresponding to the smallest values of F. The ADFs listed in Table 2 are mostly in the range 1.5–2, with only few cases above 2. Such values are obtained for our models for a variety of physical conditions.

Our models show clear trends in the values of ADFs with $Z_{\rm ISM}$, while there is no obvious trend of the observed ADFs with any observed physical parameter. Note, however, that, for the extragalactic H II regions, the uncertainties in the absorption corrections (and whether they should be applied) and the fact that for most of the extragalactic objects the ADF has been determined from just a couple of lines (or line-blends) of multiplet 1 (which are very weak and difficult to measure), preclude us from excluding any of the following possibilities: i) all the extragalactic H II regions show ADFs ∼2; ii) some extragalactic H II regions have high ADFs; iii) the low-metallicity H II regions show higher (lower) ADFs. From our models, low metallicity objects are bound to show higher ADFs. Obviously, a more conclusive sample of observational data is needed to be confronted with our model predictions.

It has been commented by López-Sánchez et al. (2007) that observed ADFs are similar in a variety of H II regions in different host galaxies. They take this fact as an argument against metal-rich droplets producing the ADFs. The entire grid of our models does predict a wide range of ADF values, which seems in contradiction with the very restricted range of observed ADFs and the fact that there seems to be no correlation between them and any observed property of the H II regions (see García-Rojas & Esteban 2006). However, not all our models necessarily represent a physically plausible model. For example, the value of $Z_{\rm D}$ is certainly constrained by physical processes occuring in the superbubbles, so that only a fraction of the considered range is relevant. In this respect, we might even suggest that, in the framework of our scenario to explain the ADFs, the observed values could put constraints on the mixing of metals in the supernova bubbles. For example, the observed ADFs do not seem to depend on metallicity whereas our models would predict larger ADFs for a lower $Z_{\rm ISM}$ if all other parameters were to remain fixed. From Table 2, the values of e_*(O) do not change with metallicity. Thus, if our scenario is to explain the observed ADFs, this implies that one or more of the remaining parameters (F, $X_{\rm i}$, or $Z_{\rm D}$) must correlate with $Z_{\rm ISM}$ in such a way as to maintain a constant ADF. Indeed, one might expect a relation between $X_{\rm i}$ and $Z_{\rm ISM}$, via metallicity-dependent stellar winds which play an important role in the shaping of the ISM and therefore on determining the mass of gas that is ionized. One might also expect a relation between $Z_{\rm D}$ and $Z_{\rm ISM}$, although Silich et al. (2001) show that this relation is not a simple one.

Note that the magnitude of the biases found in our simulations obviously depend on the value adopted for η. Had we used a value of $\eta = 0.013$, a minimum value implied by the references listed in Sect. 3.2, the biases would have been very small in most cases.

4.6. Possible effects of dust

In our models we did not consider the effect of dust. This was on purpose, in order not to inflate the number of free parameters. One of the expected effects of dust would be to decrease the amount of O available to produce recombination lines in droplets if a significant fraction of the O atoms in drops are depleted onto refractory dust grains. However, maximum dust condensation efficiencies in SNe ejecta seem to be ∼0.2 (Todini & Ferrara 2001; Edmunds 2001), so the effective value of X(O), would only decrease to by a factor of 0.8. We believe that the main effects of dust grains in this problem is their contribution to heat the gas. The efficiency of grain heating depends essentially on the dust-to-gas mass ratio, the ionization parameter, and the size of the grains. The contribution of grains to the total heating budget is larger for higher ionization parameters (Stasinska & Szczerba 2001). Since the droplets are to be denser than the surrounding gas, the ionization parameter there is lower, and therefore the effect of grain heating is expected to be smaller than in the surrounding gas. Thus, the effect of the ionization parameter alone would be to enhance the contrasts between droplets and the rest, and thus to enhance the effects discussed in the preceding section. However, the properties of the dust grains are likely very different in the droplets and in the interstellar medium, since the dust in the droplets should be heavily weighted by the conditions during the supernova ejection and droplet condensation. This issue obviously merits further study.

4.7. The abundance bias

It is often said that abundances derived from recombination lines are not biased, because all recombination lines have roughly the same temperature-dependence (e.g., Esteban et al. 2005). On the other hand, abundances derived from collisionally excited lines could be underestimated if large temperature fluctuations in the O^{++} zone are present but not accounted for. Some authors apply various techniques to try to estimate temperature fluctuations in a given object and correct for them using the scheme of Peimbert (1967). Others do not apply such a correction, considering that temperature fluctuations are expected to be small.

In the case of our scenario, the *real* metallicity is that of the fully mixed H II region. Figures 4e and 5e show that the bias $Z_{\rm CEL}/Z_{\rm HII}$ is larger than 1 in all the cases shown here. Obviously, in our scenario, one cannot expect the abundance measured from collisionally excited lines to measure the *real* metallicity exactly. The discussion of the abundance bias is unfortunately complicated by the fact that one should also consider the O^+ zone, and that the results are expected to strongly depend on the excitation of the object. We note that, in our models, the bias $Z_{\rm CEL}/Z_{\rm HII}$ is usually small, but it may reach 0.2–0.3 dex if the weight of the well-mixed H II region is small and if $Z_{\rm D}$ is of the order of 2 $Z_\odot$. It is interesting to note that this bias is opposite to the bias due to the temperature fluctuations postulated by Peimbert (1967). However, many more numerical experiments would be needed to consider this as a general rule.

Figures 4f and 5f show that the bias $Z_{\rm ORL}/Z_{\rm HII}$ is always larger than one, and may reach quite large factors. As expected, the bias increases with ADF(O^{++}).

To summarize, if the droplet scenario is valid, ORLs overestimate the *real* metallicity of the ISM, possibly by quite

large amounts. CELs may also overestimate it, although to a much weaker extent. The biases are stronger for larger ADFs. Unfortunately, we have at present no recipe to correct for the biases. In the meantime, a prudent attitude would be to discard objects with large ADFs as probes for chemical evolution studies of galaxies.

5. Conclusions and future directions

In this paper, we have described a scenario for the enrichment of the ISM and discussed its observational signatures. The scenario invokes metal-rich droplets produced by a long process following supernova explosions in previous stellar generations. The full enrichment of the ISM is only achieved when these droplets are destroyed by diffusion in photoionized regions. Following Larson (1996), if the total star formation rate in the galaxy is about 3 $M_\odot$ yr^{-1} and the amount of cloud matter that can be ionized per every solar mass converted into stars amounts to $\sim$10 $M_\odot$, then if the total gaseous mass of the galaxy amounts to 4×10^9 $M_\odot$, the ionization rate implies that the entire ISM is cycled through the ionized phase every 100 Myr. It is then within such a short timescale that the ISM acquires, at least locally, an even metallicity. On the other hand, the time required to disperse the metals from a stellar generation is much longer (several $\times 10^8$ yr, due mostly to a slow cooling process) and a significant fraction of the mass converted into stars in the last few stellar generations, which ends up being violently reinserted into the ISM, remains hidden within the hot phase of the ISM.

We have shown in Sect. 4 that photoionization of highly metallic droplets can, under certain conditions, reproduce the observed abundance discrepancy factors (ADFs) derived for Galactic and extragalactic H II regions. In this scenario the recombination lines arise from the highly metallic droplets that have not yet fully mixed with the ISM gas. However, we find in Sect. 2.2 that the droplets in H II regions can only have a narrow range of sizes, bounded from below by the need to avoid rapid destruction and from above by the need to have eluded detection by direct imaging.

We find in Sect. 4.7 that, if this scenario holds, the recombination lines strongly overestimate the metallicities of the fully mixed H II regions. The collisionally excited lines may also overestimate them, although in much smaller proportion (less than 0.1 dex in most of the cases considered in this study). The effect increases with ADF(O^{++}). In absence of any recipe to correct for these biases, we recommend that objects showing large ADFs should be discarded when probing the chemical evolution of galaxies.

From our model, we do not expect a large difference between the abundance of the fully mixed H II region (reasonably well approximated by the abundances derived from CELs) and the general ISM. On the other hand, ISM abundances as measured by absorption lines are not likely to be significantly affected by the presence of metal-rich droplets. On the other hand, the amount of O depletion of dust in the neutral ISM and in HII regions could be different, being more important in the neutral ISM than in ionized gas. Present determinations of the gaseous O/H in the solar vicinity from CELs in HII regions (Deharveng et al. 2000) and from neutral absorption lines (Meyer et al. 1998; Jensen et al. 2005) give similar values.

In order to proceed further with this question of small-scale abundance inhomogeneities, which is complicated and involves many parameters, one needs as many observational constraints as possible.

- A systematic search for ADFs for several elements (N, Ne) in the same regions would be welcome. If the droplet scenario is valid, ratios of ADFs for several elements in the same region should be in agreement with the prediction of current theories of nucleosynthesis in massive stars. On the other hand, if nitrogen is mainly produced by intermediate mass stars, the nitrogen abundance should not be greatly enhanced in the droplets we consider. The measurement of nitrogen recombination lines is crucial to test our scenario.
- A systematic search for ADFs in regions of different metallicities would be useful.
- Our simulations predict that values of ADF(O^{++}) are significantly larger than one only in specific cases. So far, ADFs have been measured in only a handful of H II regions. It would be advisable to have a much larger number of relevant observations, and to be able to relate the values of the ADFs with other properties of the H II regions and with the observing conditions (e.g. whether the slit encompasses a significant fraction of an H II region or whether the observed fluxes are heavily weighted by zones close to the ionization front). It would be very useful to have an observational census of the cases where the ADFs are close to one. This implies the systematic publication of intensities (or upper limits) of recombination lines in high signal-to-noise spectra.
- Reliable measurements of ADF(O^+) would also be important to constrain the models. At present, there are a few measurements of ADF(O^+) in H II regions, but they are highly uncertain since they rely on one or two weak lines from multiplet 1 at $\lambda \sim 7774$ Å (the brightest multiplet expected to arise completely from recombination), which are severely affected by blends with telluric features.
- Observational diagnostics of densities and temperatures from recombination lines, such as those proposed by Tsamis et al. (2004) or Liu et al. (2006) should be useful to constrain the problem (see García Rojas & Esteban 2006, for a first attempt in this direction).
- Another useful diagnostic is the temperature derived from the Balmer or Paschen jump. Recently, Guseva et al. (2006) have estimated the Balmer jump temperature in about 50 metal-poor H II galaxies. They find that the Balmer jump temperatures are similar to the [O III] λ4363/5007 temperatures, contrary to what is found in some nearby or more metal-rich H II regions (González-Delgado et al. 2004; García-Rojas et al. 2004). The interpretation of this result in the framework of the droplet scenario requires a more complicated modelling than that presented here, and is out of the scope of the present paper. We just checked by hand on a few cases that, in our scenario, it is possible to obtain values of the Balmer jump temperatures equal to (or even slightly higher than) the [O III] λ4363/5007 temperatures, depending on the fraction of [O III] λ4363 and [O III] λ5007 light coming from the droplets. This question obviously requires further analysis.

A large amount of observational work thus remains to be done to improve our understanding of the conditions in which intimate mixing occurs in the ISM.

On the theoretical side, many questions remain unsettled. For example, no firm theoretical prediction exists for the droplet mass spectrum, which would allow comparison with the constraints on droplet sizes that we derive in Sect. 2.2. Furthermore, one needs to better understand the properties of turbulence in H II regions since, in order for the droplets to survive long enough to explain the observed ADFs, it is vital that the regions not be

too turbulent. The question of the survival of the droplets in the neutral/molecular ISM is another question that needs addressing. The photoionization models currently rely on several free parameters that are not well-constrained by observations: one needs more robust estimates of the integrated stellar yields as well as a better understanding of the impact of massive stars on the ISM.

Given the relevance of all these issues to our understanding of the chemical evolution of galaxies, this subject deserves to be explored much further than we have been able to do in this paper.

Acknowledgements. This work started from discussions between G.S., G.T.T. and M.R. at the Guillermo Haro Workshop, at INAOE Puebla, in July 2004. GTT acknowledges financial support from the Secretaría de Estado de Universidades e Investigación (España) through grant SAB2004-0189 and from the Université de Paris 7 and the hospitality provided by the Instituto de Astrofísica de Andalucía (IAA, CSIC) in Granada, Spain, and also by the Observatoire de Paris Meudon, France. G.S. aknowledges the hospitality of the INAOE. WJH acknowledges support from DGAPA-UNAM, through project PAPIIT 112006-3. We thank Georges Alecian and Franck Le Petit for discussions, Bob Rubin and Yiannis Tsamis for their comments on a first version of the manuscript. Finally, we are very grateful to the referee as well as to Malcom Walmsley for their insightful comments which helped to improve the paper significantly.

References

Allende Prieto, C., Lambert, D. L., & Asplund, M. 2001, ApJ, 556, L63
Aloisi, A., Savaglio, S., Heckman, T. M., et al. 2003, ApJ, 595, 760
Bateman, N. P., & Larson, R. B. 1993, ApJ, 407, 634
Chiappini, C., Romano, D., & Matteucci, F. 2003, MNRAS, 339, 63
de Avillez, M. A., & Mac Low, M.-M. 2002, ApJ, 581, 1047
Deharveng, L., Peña, M., Caplan, J., & Costero, R. 2000, MNRAS, 311, 329
Devost, D., Roy, J-R., & Drissen, L. 1997, ApJ, 482, 765
Edmunds, M. G. 2001, MNRAS, 328, 223
Esteban, C., Peimbert, M., Torres-Peimbert, S., & Escalante, V. 1998, MNRAS, 295, 401
Esteban, C., Peimbert, M., Torres-Peimbert, S., García-Rojas, J., & Rodríguez, M. 1999a, ApJS, 120, 113
Esteban, C., Peimbert, M., Torres-Peimbert, S., & García-Rojas, J 1999b, Rev. Mex. A&A, 35, 65
Esteban, C., Peimbert, M., Torres-Peimbert, S., & Rodríguez, M. 2002, ApJ, 581, 241
Esteban, C., Peimbert, M., García-Rojas, J., et al. 2004, MNRAS, 355, 229
Esteban, C., García-Rojas, J., Peimbert, M., et al. 2005, ApJ, 618, L95
Franco, J., Shore, S., & Tenorio-Tagle, G. 1994, ApJ, 436, 795
François, P., Matteucci, F., Cayrel, R., et al. 2004, A&A, 421, 613
García-Segura, G., & Franco, J. 1996, ApJ, 469, 171
García-Rojas, J., & Esteban, C. 2006, in Highlights of Spanish Astrophysics IV, Proceedings of the VII Scientific Meeting of the Spanish Astronomical Society [arXiv:astro-ph/0610903]
García-Arredondo, Henney, & Arthur, S. J. 2001, ApJ, 561, 830
García-Rojas, J., Esteban, C., Peimbert, M., et al. 2004, ApJS, 153, 501
García-Rojas, J., Esteban, C., Peimbert, M., et al. 2005, MNRAS, 362, 301
García-Rojas, J., Esteban, C., Peimbert, M., et al. 2006a, MNRAS, 368, 253
García-Rojas, J., Esteban, C., Peimbert, A., et al. 2006b, Rev. Mex. Astron. Astrofis., in press
González-Delgado, R. M., Enrique, P., Guillermo, T.-T., et al. 1994, ApJ, 437, 239
Guseva, N. G., Izotov, Y. I., & Thuan, T. X. 2006, ApJ, 644, 890
Henney, W. J. 2003, in Winds, bubbles, and explosions: a conference to honor John Dyson, ed. S. J. Arthur, & W. J. Henney, Rev. Mex. Astron. Astrofis. Ser. Conf., 15, 175
Henney, W. J. 2006, in Diffuse Matter from Star Forming Regions to Active Galaxies: A Volume Honouring John Dyson, ed. T. W. Harquist, J. M. Pittard, & S. A. E. G. Falle (Dordrecht: Springer), in press [arXiv:astro-ph/0602626]
Henney, W. J., Arthur, S. J., & García-Díaz, M. T. 2005, ApJ, 627, 813
Henry, R. B. C., Edmunds, M. G., & Köppen, J. 2000, ApJ, 541, 660
Jensen, A. G., Rachford, B. L., & Snow, T. P. 2005, ApJ, 619, 891
Kahn, F. D. 1991 in The interstellar disk-halo connection in galaxies, ed. H. Bloemen (Kluwer Academic Press), 1
Klessen, R. S., & Lin, D. N. 2003, Phys. Rev. E, 67, 04631
Kniazev, A. Y., Grebel, E. K., Pustilnik, S. A., Pramskij, A. G., & Zucker, D. B. 2005, AJ, 130, 1558
Kobulnicky, H. A., & Skillman, E. 1996, ApJ, 471, 211
Kobulnicky, H. A., Skillman, E. D., Roy, J.-R., Walsh, J. R., & Rosa, M. R. 1997, ApJ, 477, 679
Kroupa, P. 2001, MNRAS, 322, 231
Lanfranchi, G. A., & Matteucci, F. 2003, MNRAS, 345, 71
Larson, R. 1996 in The interplay between massive stars the ISM and galaxy evolution, ed. D. Kunth, B. Guiderdoni, M. Heydari-Malayeri, & T. X. Thuan, (Editions Frontieres), 3
Lebouteiller, V., Kunth, D., & Lequeux, J., A. 2004, A&A, 415, 55
Legrand, F. 2000, NewAR, 44, 345
Liu, X.-W., Storey, P. J., & Barlow, M. J. 2000, MNRAS, 312, 585
Liu, Y., Liu, X.-W., Barlow, M. J., & Luo, S.-G. 2004, MNRAS, 353, 1251
Liu, X.-W., Barlow, M. J., Zhang, Y., Bastin, R. J., & Storey, P. J. 2006, MNRAS, 404
López-Sánchez, A. R., Esteban, C., García-Rojas, J., Peimbert, M., & Rodríguez, M. 2007, ApJ, 656, 168
McKee, C. F., & Williams, J. P. 1997, ApJ, 476, 144
Mellema, G., Arthur, S. J., Henney, W. J., Iliev, I. T., & Shapiro, P. R. 2006, ApJ, 647, 397
Meyer, D. M., Jura, M., & Cardelli, J. A., 1998, ApJ, 493, 222
Mollá, M., & Díaz, A. I. 2005, MNRAS, 358, 521
O'Dell, C. R., & Castañeda, H. O. 1987, ApJ, 317, 686
O'Dell, C. R., Peimbert, M., & Peimbert, A. 2003, AJ, 125, 2590
Oey, M. S. 2003, MNRAS, 339, 849
Pan, L., & Scalo, J. 2007, ApJ, 654, L29
Peimbert, M. 1967, ApJ, 150, 825
Peimbert, A. 2003, ApJ, 584, 735
Peimbert, M., Storey, P. J., & Torres-Peimbert, S. 1993, ApJ, 414, 626
Peimbert, A., Peimbert, M., & Ruiz, M. T. 2005, ApJ, 634, 1056
Portinari, L., Chiosi, C., & Bressan, A. 1998, A&A, 334, 505
Roy, J-R., & Kunth, D. 1995, A&A, 294, 432
Różyczka, M., & Tenorio-Tagle, G. 1985, Acta Astron., 35, 213
Rubin, R. H., Martin, P. G., Dufour, R. J., et al. 2003, MNRAS, 340, 362
Salpeter, E. E. 1955, ApJ, 121, 161
Scalo, J. M. 1986, FCPh, 11, 1
Scalo, J., & Elmegreen, B. G. 2004, ARA&A, 42, 275
Schiano, A. V. R., Christiansen, W. A., & Knerr, J. M. 1995, ApJ, 439, 237
Silich, S., Tenorio-Tagle, G., Terlevich, R., Terlevich, E., & Netzer, H. 2001, MNRAS, 324, 191
Simón-Díaz, S., Herrero, A., Esteban, C., & Najarro, F. 2006, A&A, 448, 351
Stasińska, G. 2005, A&A, 434, 507
Stasinska, G., & Leitherer, C. 1996, ApJS, 107, 661
Stasińska, G., & Szczerba, R. 2001, A&A, 379, 1024
Stasińska, G., Tenorio-Tagle, G., Rodríguez, M., & Henney, W. J. 2007, in The Metal-Rich Universe, ed. G. Israelian, & G. Meynet (Cambridge University Press), in press [arXiv:0704.0160]
Tenorio-Tagle, G. 1979, A&A, 71, 59
Tenorio-Tagle, G. 1996, AJ, 111, 1641 (T-T96)
Thuan, T. X., Lecavelier des Etangs, A., & Izotov, Y. I. 2005, ApJ, 621, 269
Todini, P., & Ferrara, A. 2001, MNRAS, 325, 726
Torres-Peimbert, S., Peimbert, M., & Peña, M. 1990, A&A, 233, 540
Tsamis, Y. G., & Péquignot, D. 2005, MNRAS, 364, 687
Tsamis, Y. G., Barlow, M. J., Liu, X.-W., Danziger, I. J., & Storey, P. J. 2003, MNRAS, 338, 687
Tsamis, Y. G., Barlow, M. J., Liu, X.-W., Storey, P. J., & Danziger, I. J. 2004, MNRAS, 353, 953
Vietri, M., & Pesci, E. 1995, ApJ, 442, 618
Vílchez, J. M., & Iglesias-Páramo, J. 1998, ApJ, 508, 248
Walsh, J. R., & Roy, J.-R. 1989, MNRAS, 239, 297
Williams, R. J. R. 1999, MNRAS, 310, 789
Williams, R. J. R. 2002, MNRAS, 331, 693
Williams J. P., & McKee, C. F. 1997, ApJ, 476, 166
Woosley, S. E., & Weaver, T. A. 1995, ApJS, 101, 181
Zel'dovich, Ya. B., & Raizer, Ya. P. 1966, in Physics of shock waves and high temperature hydrodynamic phenomena (New York: Academic Press)